PHYSICAL REVIEW MATERIALS **1**, 034601 (2017)

Strong effect of electron-phonon interaction on the lattice thermal conductivity in 3C-SiC

Tianshi Wang, Zhigang Gui, Anderson Janotti, and Chaoying Ni
Department of Materials Science and Engineering, University of Delaware, Newark, Delaware 19716, USA

Prashant Karandikar
M-Cubed Technologies, Inc., Newark, Delaware 19711, USA
(Received 19 May 2017; published 3 August 2017)

3C-SiC is a promising semiconductor for many applications where doping and heat dissipation are fundamental parameters in the device design. However, the variation of thermal conductivity with carrier concentration remains to be explored. Using density functional theory, we computed the lattice thermal conductivity in intrinsic and doped 3C-SiC with charge carrier concentrations in the range of 10^{17} to 10^{21} cm^{-3}. From the calculated phonon dispersion, group velocities, and phonon-phonon scattering rates for undoped bulk 3C-SiC, we obtain a thermal conductivity of 491 W/m K at 300 K. In the case of doped 3C-SiC, we find that the lattice thermal conductivity is strongly reduced at high carrier concentrations. We also predict the effects of electron-phonon interaction (EPI) to be much stronger for hole- than electron-doped material, which is explained by the features of the electronic band structure near the band edges. In the limit of high carrier concentration of 10^{21} cm^{-3}, the thermal conductivity drops by 57% for hole and 32% for electron doping. Our results and analysis provide an in-depth understanding of phonon transport for the design of novel SiC-based electronics.

DOI: 10.1103/PhysRevMaterials.1.034601

I. INTRODUCTION

SiC combines a series of desired properties for high-power electronic applications, such as wide band gap [1], high thermal conductivity, and high breakdown voltage [2]. Among the many existing polytypes, 3C-SiC has the simple isotropic zinc blende crystal structure. 3C-SiC has several advantages compared to other polytypes. It can grow heteroepitaxially on silicon substrates [3] and is a promising material for mechanical and thermal sensors [4]. 3C-SiC is also used to fabricate light-emitting diodes [5] and serves as a substrate in the growth of graphene [6]. The lattice thermal conductivity of 3C-SiC is an important parameter not only for high power devices, but also for substrate temperature control and uniformity during epitaxial growth and for device packaging design.

Experimental data for thermal conductivity in intrinsic or doped 3C-SiC are scarce, in part due to the difficulty of growing crystals with high structural quality [7]. Morelli *et al.* [8] obtained a value of 330 W/m K at room temperature for a polycrystalline sample, and suggested that their result is limited by scattering from grain boundaries. This value is much lower than those reported for the structurally more complex hexagonal 4H- or 6H-SiC polytypes [9,10]. Since in many applications of interest the 3C-SiC is doped with high carrier densities, of 10^{19} cm^{-3} or even 10^{21} cm^{-3} [4,11], it is essential to understand the role of the electron-phonon interaction on the thermal conductivity of electron- and hole-doped SiC. Both theory [12] and experiments [13] reveal that the impact of electron-phonon interaction on the thermal conductivity in silicon is significant at room temperature. Such an effect has not yet been investigated for SiC.

Here we use first-principles calculations to predict the heat transport properties in intrinsic and doped SiC. Due to the limitation in computational resources, this study focuses on 3C-SiC. Calculations for 4H- and 6H-SiC would require much more computational effort due to a larger number of atoms in the primitive cell. However, we believe our results also apply to these other SiC polymorphs, due to the similarities in crystal structure, especially in the in-plane directions of the hexagonal 2H, 4H, and 6H polytypes. The approach offers the advantage of being free of any adjustable parameters and has a general applicability. In the following, we describe the details of the calculations, present the results for the phonon dispersion, the phonon-phonon scattering, and the lattice thermal conductivity in intrinsic SiC. We then present the calculated electron-phonon scattering rates, and predict the impact of the carrier concentration on thermal conductivity for electron- and hole-doped 3C-SiC. The effect of phonon scattering with natural Si and C isotopes is included in all the calculations.

II. COMPUTATIONAL APPROACH

The intrinsic thermal conductivity tensor can be solved iteratively using the Boltzmann transport equation (BTE) [14]

$$\kappa^{\alpha\beta} = \frac{1}{k_B T^2 \Omega N} \sum_{\lambda} n_\lambda^0 (n_\lambda^0 + 1)(\hbar\omega_\lambda)^2 v_\lambda^\alpha v_\lambda^\beta \tau_\lambda, \qquad (1)$$

where α and β are the cartesian components, Ω is the volume of the primitive cell, and N denotes the number of q points in a grid used to sample the Brillouin zone; λ denotes a phonon mode with polarization v and wave vector $\mathbf{q}$, ω_λ is the angular frequency for the phonon mode λ, and n_λ^0 is the Bose-Einstein distribution function; v_λ^α is the projection of the phonon group velocity along the direction α. Finally, τ_λ denotes the phonon lifetime, which is the inverse of the scattering rate Γ_λ. The scattering rate contains the contributions from the phonon-phonon scattering, isotopic effect, EPI, etc., as described by the Matthiessen's rule.

The phonon-phonon scattering which is the dominant factor in intrinsic thermal conductivity is calculated based on the density functional theory (DFT) [15,16] and the

 ©2017 American Physical Society

density functional perturbation theory (DFPT) [17,18]. We first calculate the second order interatomic force constants (IFCs) from DFPT and obtain the phonon frequency and group velocity for each phonon in a grid. The third order IFCs are derived using the finite difference method from a set of force-displacement data obtained from DFT calculations. With the third order IFC, we obtain the scattering matrix elements $V_{\lambda\lambda'\lambda''}$ as described in Ref. [14]. We then solve the three-phonon scattering rates $\Gamma^{\pm}_{\lambda\lambda'\lambda''}$ from the Fermi's golden rule as [14,19]

$$\Gamma^{\pm}_{\lambda\lambda'\lambda''} = \frac{\hbar\pi}{4}\begin{Bmatrix} n' - n'' \\ n' + n'' + 1 \end{Bmatrix}\frac{\delta(\omega \pm \omega' - \omega'')}{\omega\omega'\omega''}|V^{\pm}_{\lambda\lambda'\lambda''}|^2, \quad (2)$$

where the upper (lower) row in the curly brackets follows the + (−) sign, which corresponds to the absorption (emission) processes. n' stands for $n^0_{\lambda'}$, and so forth. The effect of isotopic disorder on the phonon scattering rate in intrinsic SiC is included using the Matthiessen's rule as described in Ref. [19] taking the Si and C natural isotopic distributions from Ref. [20].

The thermal conductivity of the doped material is calculated by incorporating the phonon scattering rate due to the EPI, which is related to the imaginary part of the phonon self-energy, and is calculated using Fermi's golden rule as [21,22]

$$\frac{1}{\tau^{\text{ph}}_{\mathbf{q}\nu}} = \frac{2\pi}{\hbar}2\sum_{mn}\int\frac{d\mathbf{k}}{\Omega_{\text{BZ}}}|g_{mn\nu}(\mathbf{k},\mathbf{q})|^2(f_{n\mathbf{k}} - f_{m\mathbf{k}+\mathbf{q}}) \times \delta(\varepsilon_{m\mathbf{k}+\mathbf{q}} - \varepsilon_{n\mathbf{k}} - \hbar\omega_{\mathbf{q}\nu}), \quad (3)$$

where Ω_{BZ} is the volume of the Brillouin zone, and $f_{n\mathbf{k}}$ is the distribution function for electrons. The factor of 2 before the summation accounts for the spin degeneracy. The matrix element $g_{mn\nu}(\mathbf{k},\mathbf{q})$ of one electron-phonon scattering process involves a phonon with polarization ν and two electrons with band indices m and n. It can be derived from DFPT using $g_{mn\nu}(\mathbf{k},\mathbf{q}) = \frac{1}{\sqrt{2\omega_{\mathbf{q}\nu}}}\langle\psi_{m\mathbf{k}+\mathbf{q}}|\partial_{\mathbf{q}\nu}V|\psi_{n\mathbf{k}}\rangle$ [23]. Note that the phase changes after scattering should not change the value of $|g_{mn\nu}(\mathbf{k},\mathbf{q})|^2$ and the derived scattering rates. The calculations are quite computationally consuming because a proper description of the scattering processes requires convergence using very fine meshes in the Brillouin zone. To lower the computational cost, we employ the recently developed interpolation techniques based on maximally localized Wannier function (MLWF) transformation [22,24,25] which have successfully provided accurate results for other materials [23,25]. We then derive the phonon scattering rates for each mode using the Matthiessen's rule by combining the results from the electron-phonon interaction and the results from iteratively solving for the intrinsic material. Finally, we obtain the thermal conductivity of doped materials using Eq. (1).

We use the Quantum ESPRESSO package [26] for the DFT and DFPT calculations, within the local density approximation (LDA) [27]. Norm-conserving pseudopotentials [28] and a plane wave cutoff of 100 Ry are employed. We first perform structural optimization using a $12 \times 12 \times 12$ **k**-point mesh (**k** mesh). The convergence tolerance of total energy is set to 10^{-12} Ry. The calculated equilibrium lattice parameter is 4.342 Å, in good agreement with the experimental value of 4.360 Å [29]. In the phonon calculations, the dynamic matrices and second order IFCs are computed on a $6 \times 6 \times 6$ **q**-point mesh (**q** mesh). In the third order IFCs calculations, a cutoff of 5.025 Å (or up to the fifth nearest-neighbor atoms) is chosen for the interaction range after comparing with the results using 4.537 Å (i.e., up to the fourth nearest-neighbor atoms). We generate 204 displaced supercells, each with 250 atoms, with the atomic displacements of 0.021 Å. The ShengBTE package [19] is used for obtaining the third order IFCs and for solving the phonon Boltzmann transport equation (BTE) iteratively. When solving the BTE, we performed convergence tests with respect to the **q** mesh. Tests using **q** meshes of $40 \times 40 \times 40$ and $35 \times 35 \times 35$ give less than 0.5% differences. For convenience, we choose the latter as **q** mesh size. We also repeated the calculations using the generalized gradient approximation of Perdew-Burke-Ernzerhof for the exchange-correlation term [30] and find changes in thermal conductivity of less than 2% at room temperature.

Finally, we calculate the EPI for electron and hole concentrations varying from 10^{17} to 10^{21} cm^{-3}. The EPW code [23] is used to interpolate the EPI matrices as well as the electron and phonon eigenvalues from the coarse to the fine meshes. We chose a **q** mesh of $35 \times 35 \times 35$, the same as in the phonon-phonon scattering calculations. We set the **k** mesh to $120 \times 120 \times 120$ and the Gaussian broadening to 2 meV. This gives less than 0.5% difference compared to results using $144 \times 144 \times 144$ and 1 meV.

III. RESULTS AND DISCUSSION

A. Phonon dispersion and electronic structure

The calculated phonon dispersion of 3C-SiC is shown in Fig. 1(a), in comparison with experimental data [31,32]. We find a gap of 3.5 THz between the highest acoustic phonon frequency and the lowest optical phonon frequency, in good agreement with the experimental results [31]. Such a gap inhibits three-phonon scattering processes involving optical and acoustic modes because of the energy and quasimomentum conservation requirements, thus leading to longer phonon lifetimes. Figure 1(b) shows the phonon density of states (DOS) and atom-resolved DOS. The three acoustic phonon branches at low frequencies are associated mostly with Si due to its heavier atomic mass, while the three optical branches at frequencies higher than 20 THz are associated with C.

The electronic band structure of 3C-SiC is shown in Fig. 1(c). The gap is indirect with the valence-band maximum at Γ and conduction-band minimum at X. The calculated band gap is 1.36 eV, compared to the experimental value of 2.36 eV [33]. This large error is due to the DFT-LDA deficiency in describing band gaps; by no means will it affect our conclusions regarding the effects of carriers on the thermal conductivity since the transitions across the gap do not contribute in our analysis. The electronic density of states is shown in Fig. 1(d). It shows that the density of states for holes is significantly larger than that for electrons, and this will have important consequences for the effects of EPI on the thermal conductivity as discussed later in the text.

B. Phonon scattering and lattice thermal conductivity in intrinsic SiC

The calculated lattice thermal conductivity (κ) of bulk 3C-SiC, including the isotopic effect, is shown in Fig. 2(a)

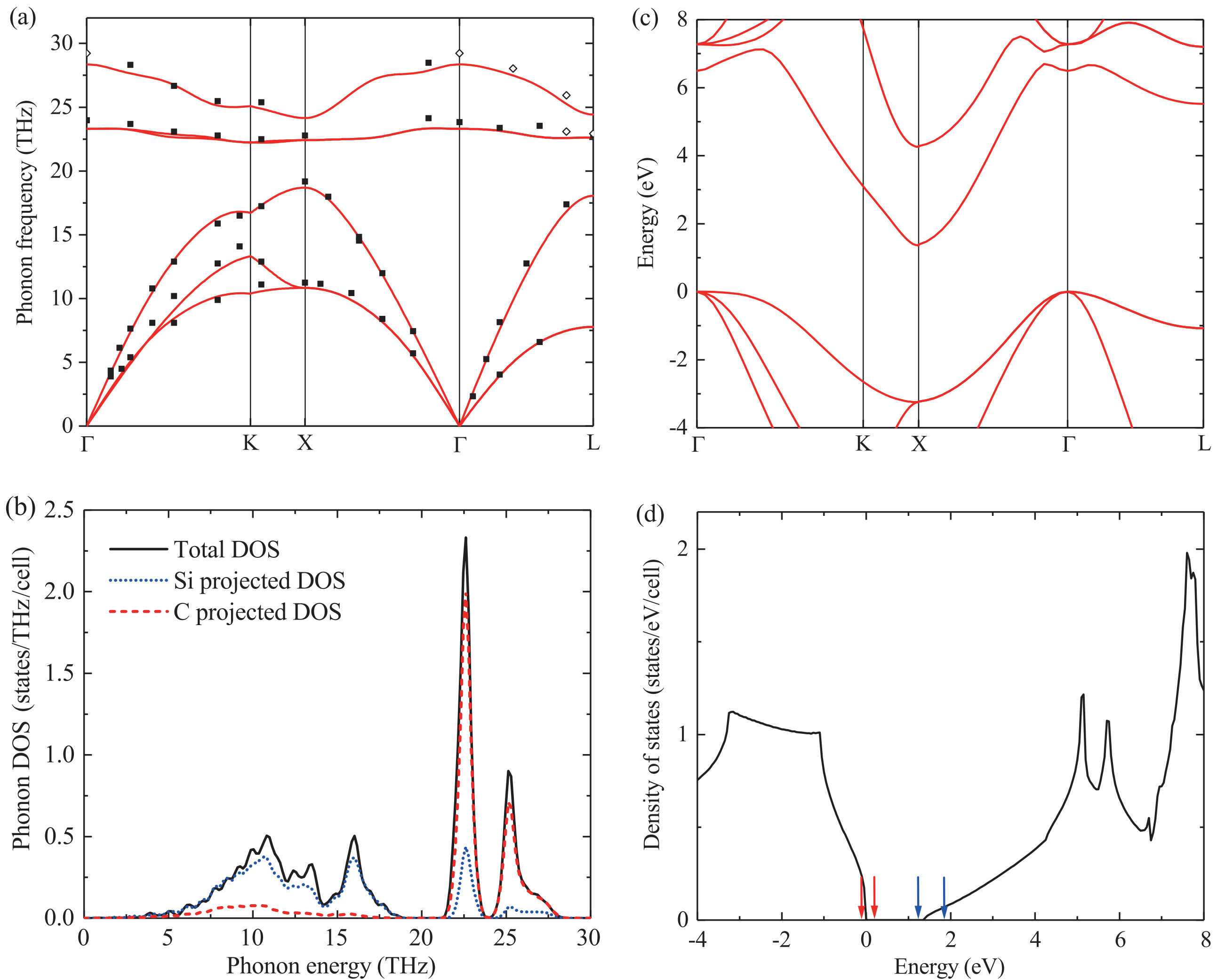

FIG. 1. Phonon dispersion and electronic band structure of 3C-SiC. (a) Calculated phonon dispersion along with the experimental data (filled squares) from Ref. [31] and (open diamonds) from Ref. [32]. (b) Total phonon density of states (black) and atom-resolved DOS: Si (blue) and C (red). (c) Calculated electronic band structure showing the indirect gap at Γ-X and (d) the total density of states near the valence- and conduction-band edges. We place the zero at the top of the valence band. The position of the Fermi levels for electron (blue) and hole (red) concentrations of 10^{17} and 10^{21} cm^{-3} is indicated with arrows in (d).

along with experimental results [8,10,34]. At 300 K we find κ is 491 W/m K, close to previous calculation of 479 W/m K [35]. We note that the theoretical results are higher than the experimental values of Taylor [34] and Morelli [8]. This difference may be related to the crystalline quality of the samples. For example, the results of Morelli *et al.*, as the authors suggest, are affected by scattering from grain boundaries [8]. Therefore, it is reasonable that our results for undoped bulk crystal end up higher than their experimental values, especially at low temperatures where scattering by grain boundaries and other defects dominates. At elevated temperatures, where phonon-phonon scattering dominates heat transport in intrinsic semiconductors, the calculated results match well with the experimental values. We also find good agreement between our results for 3C-SiC and the experimental values for 6H-SiC with N concentration of $\sim 10^{17}$ cm^{-3} [10], where accurate in-plane results are available. This is expected, since the local lattice configurations of 3C-SiC and 6H-SiC are quite similar.

It is interesting to analyze how much each phonon branch contributes to the total thermal conductivity at a given temperature. The calculated phonon-scattering rates for each of the six phonon branches at 300 K is shown in Fig. 2(b). We find that the acoustic phonons, especially low-frequency phonons, have the lowest scattering rates and therefore contribute the most to the total thermal conductivity. At 300 K, the two transverse and one longitude acoustic branches contribute 38%, 32%, and 28%, respectively. Indeed, we find that the acoustic branches dominate at every studied temperature, contributing more than 95% of the total thermal conductivity.

The phonon-resolved contribution to the total thermal conductivity can also give information on the sample size effects on the heat transport. For instance, in nanostructures or polycrystalline samples, heat transport may be limited by interface scattering. If the characteristic diameter of the nanostructure or grain is less than the maximum mean free path (MFP) of the phonons that contribute the most to the thermal conductivity, the thermal conductivity will be lower than that

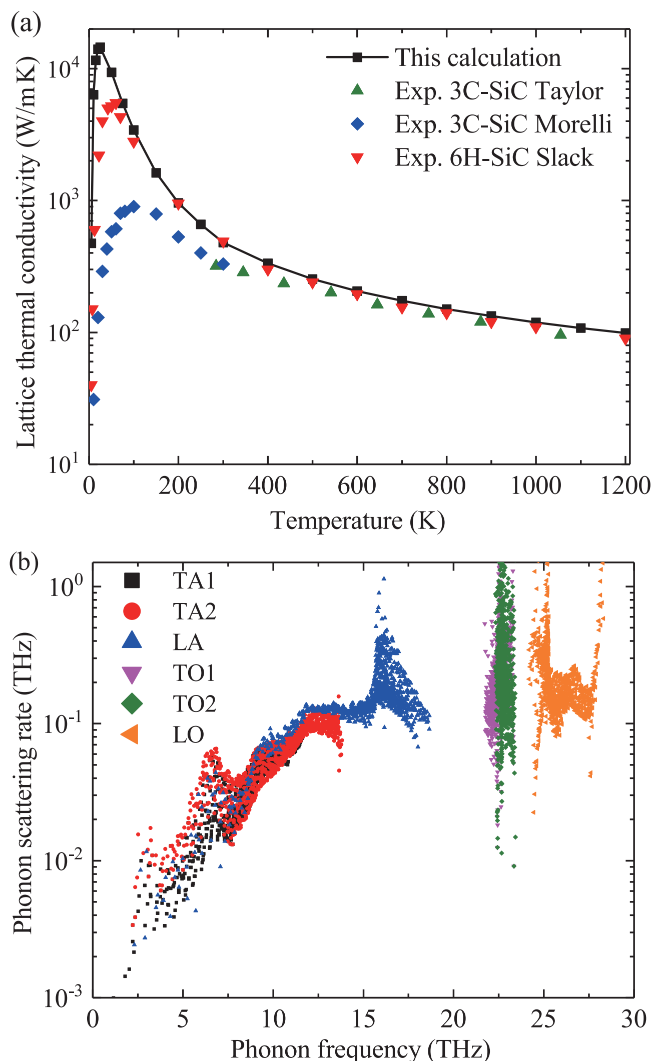

FIG. 2. (a) Calculated lattice thermal conductivity (black square and solid line) of undoped 3C-SiC as a function of temperature. The experimental values for 3C-SiC are from Ref. [8] (diamonds) and from Ref. [34] (triangles). The experimental values for 6H-SiC (inverted triangles) in the planes perpendicular to the c axis are from Ref. [10]. (b) Phonon scattering rates for the six branches in intrinsic 3C-SiC at 300 K.

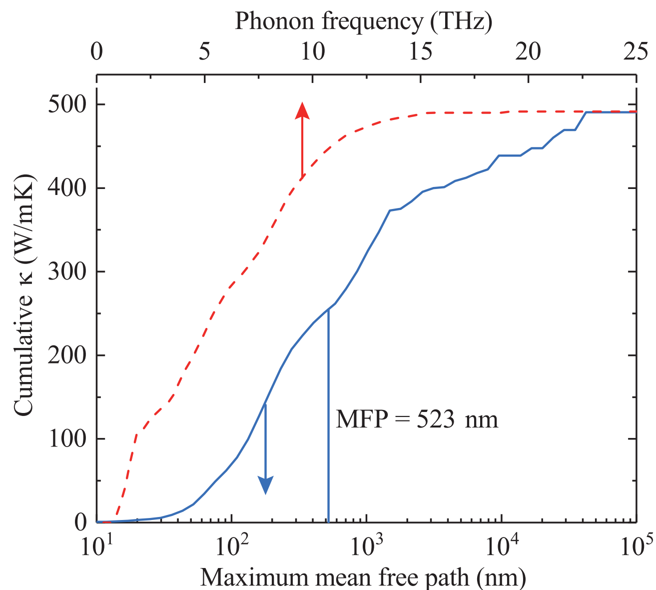

FIG. 3. Cumulative thermal conductivity of pure 3C-SiC as a function of the maximum mean free path and phonon frequency at 300 K.

of bulk at a given temperature. Figure 3 shows the cumulative thermal conductivity as a function of maximum MFP and phonon frequency at room temperature [19]. The maximum MFP of a phonon mode λ is the product of its lifetime τ_λ and the absolute value of the group velocity $|\mathbf{v}_\lambda|$. Using the method described in Ref. [19], we find that MFP of the relevant heat carriers at room temperature is around 523 nm. We also calculated the cumulative thermal conductivity as a function of phonon frequency, as shown in Fig. 3. Our results show that phonons with frequencies below 12 THz contribute 95% of the total lattice thermal conductivity in intrinsic SiC.

C. Effects of electron-phonon interaction on the thermal conductivity

Having discussed the lattice thermal conductivity in undoped SiC, we now present the results for the effects of having electrons in the conduction band or holes in the valence band on the thermal conductivity, i.e., how electron-phonon interaction affects the phonon-scattering rates. We limit this study to the effects of the carriers only, neglecting their source which can be either by introducing donor or acceptor impurities, or by light excitation where both electron and holes are created. We note that we do not consider the phonon scattering by the impurities or defects that could be the source of the carriers. This effect may also contribute to thermal conductivity in doped materials as recently discussed in Ref. [36].

First, we discuss the limit of very high carrier density. Figure 4 shows the phonon scattering rates that arise from electron-phonon interaction for carrier concentration of 10^{21} cm^{-3} in 3C-SiC at 300 K. For both electron-doped and hole-doped cases, the phonon scattering rates from EPI are comparable to those from the three-phonon processes, especially for low-frequency phonons (below 12 THz). Since the low frequency phonons contribute 95% of total thermal conductivity in intrinsic 3C-SiC, our results show that electron-phonon scattering significantly affects the thermal conductivity in 3C-SiC with high carrier concentrations.

We note that electron-phonon interaction in hole-doped 3C-SiC [Fig. 4(b)] is much stronger than that in electron-doped material [Fig. 4(a)]. This difference can be inferred from the energy and quasimomentum conservation, and the electronic structure of 3C-SiC near the band edges. Since the phonon energy is small, an electron or hole cannot transit to conduction band from valence band; therefore, its initial and final electronic states remain near the Fermi level, which resides near the valence-band edge in hole-doped or near the conduction-band edge in electron-doped materials. In 3C-SiC there are three bands near the valence-band edge, with relatively small energy differences between them. Therefore, holes can transit within a same band as well as jump between the three bands by absorbing or emitting phonons. In contrast, there is only a single band near the conduction-band edge,

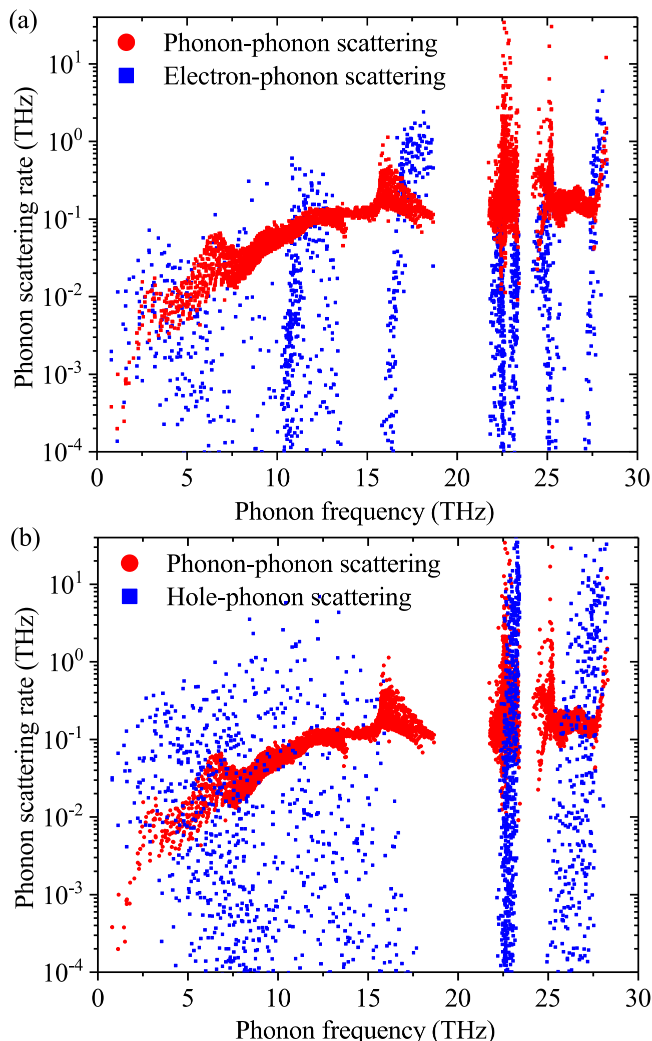

FIG. 4. Phonon scattering rates from the intrinsic phonon-phonon scattering (red cycle) and electron-phonon interaction (blue square) at 300 K in 3C-SiC with (a) electron and (b) hole concentration of 10^{21} cm^{-3}.

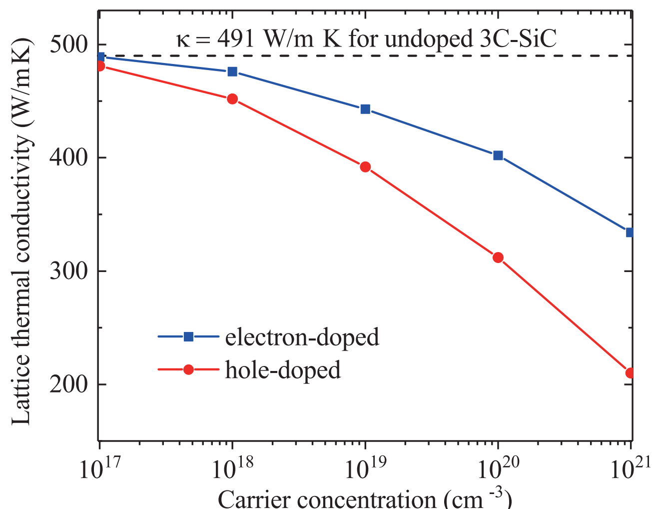

FIG. 5. The lattice thermal conductivity κ as a function of carrier concentration in 3C-SiC, taking account of phonon-phonon scattering and electron-phonon interaction (EPI).

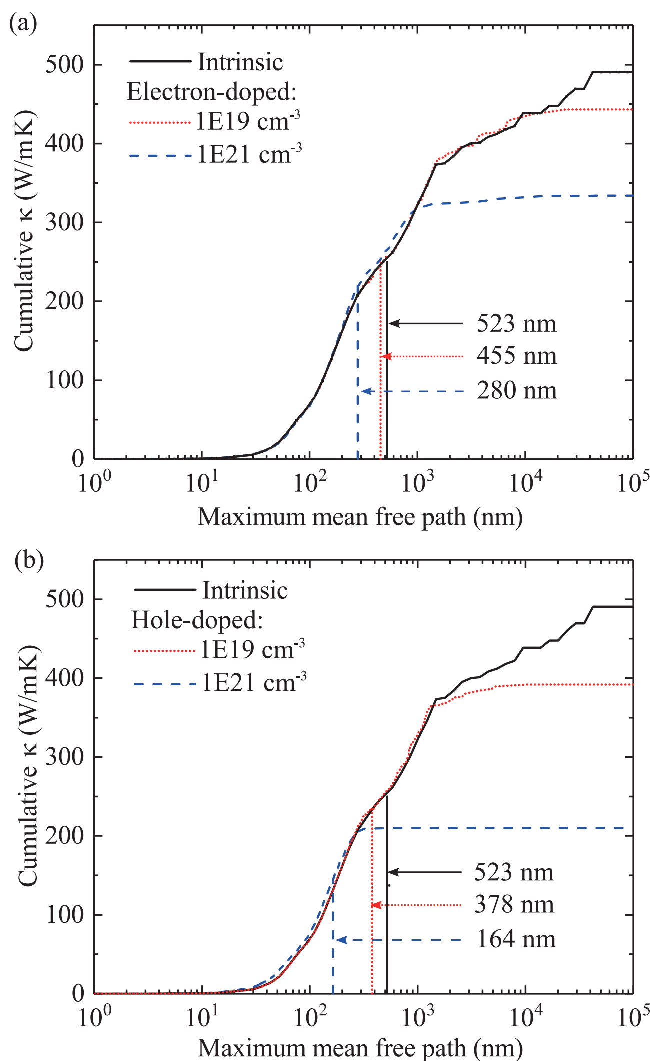

FIG. 6. Cumulative thermal conductivity of electron- and hole-doped 3C-SiC as a function of the maximum mean free path at 300 K.

and the electrons can only transit within this single band. In addition, as shown in Fig. 1(c) the curvature of the bands near valence-band edge is lower than that of the conduction-band edge, i.e., the effective masses of the holes are higher than that of the electrons [37], translating into higher density of hole states than electron states as shown in Fig. 1(d). Therefore, because of the differences of electronic structure near valence-band and conduction-band edges, electron-phonon scattering in hole-doped material is much stronger than in electron-doped material. In other words, both the degeneracy of the hole bands and the heavier hole masses lead to much higher scattering rates in hole-doped than in electron-doped 3C-SiC for the same carrier density.

The calculated lattice thermal conductivity is shown in Fig. 5 for 3C-SiC with carrier concentrations varying from 10^{17} to 10^{21} cm^{-3} at 300 K. As discussed above, we find that hole doping leads to lower thermal conductivities than electron-doped 3C-SiC. Most notably, we find a significant reduction in κ, from 491 W/m K for undoped material, to

392 and 210 W/m K, respectively, for hole concentrations of 10^{19} and 10^{21} cm^{-3}. In contrast, for the same electron concentrations we find that the thermal conductivity decreases to 443 and 334 W/m K. Recent yet unpublished work by Protik *et al.* [38] on 2H-SiC shows that the effect of EPI leads to a decrease in the lattice thermal conductivity by 1% and 4.4% for electron concentrations of 10^{17} and 10^{18} cm^{-3}, respectively, in agreement with our calculation for 3C-SiC.

The electron-phonon interaction also affects heat transport in nanostructured or polycrystalline samples, depending on their characteristic length. The cumulative thermal conductivity of electron- and hole-doped 3C-SiC as a function of the MPF at 300 K is shown in Fig. 6. With increasing electron or hole concentrations, the mean free path drops rapidly due to the strong effect of electron-phonon interaction. The calculated mean free path drops to 280 and 164 nm in electron- and hole-doped 3C-SiC, respectively, in the limit of very high carrier concentration of 10^{21} cm^{-3}.

Finally, although all our calculations were performed for the 3C-SiC polytype, we expect our results to be also valid for the 2H-, 4H-, and 6H-SiC polytypes. For instance, preliminary calculations for the lattice thermal conductivity in 2H-SiC show a very small anisotropy in the phonon-scattering rates and thermal conductivity for undoped material. Since the electronic density of states are quite similar, we also expect that the effects of carriers on the thermal transport to be similar in all these polytypes.

IV. SUMMARY AND CONCLUSIONS

We calculated lattice thermal conductivity for intrinsic as well as electron- and hole-doped 3C-SiC using first-principles methods. We predict a lattice thermal conductivity of 491 W/m K and a phonon mean free path ~523 nm at 300 K for bulk 3C-SiC. We find that electron-phonon interaction is much stronger in hole-doped than in electron-doped 3C-SiC, which is explained by the degeneracy of the valence-band edge and heavier hole masses. We predict that the room-temperature thermal conductivity significantly decreases from 491 W/m K of intrinsic material to 210 and 334 W/m K in the limit of high hole and electron concentrations of 10^{21} cm^{-3}.

ACKNOWLEDGMENTS

T.W. and C.N. gratefully acknowledge financial support from the II-VI Foundation, and A.J. is grateful for the financial support from National Science Foundation under Grant No. 1652994. This research was supported through the use of the Extreme Science and Engineering Discovery Environment (XSEDE) supercomputer facility, National Science Foundation Grant No. ACI-1053575, and the Information Technologies (IT) resources at the University of Delaware, specifically the high-performance computing resources.

[1] L. Patrick, D. R. Hamilton, and W. J. Choyke, Phys. Rev. **143**, 526 (1966).
[2] W. J. Choyke and G. Pensl, MRS Bull. **22**, 25 (1997).
[3] P. Tanner, L. Wang, S. Dimitrijev, J. Han, A. Lacopi, L. Hold, and G. Walker, Sci. Adv. Mater. **6**, 1 (2014).
[4] M. I. Lei and M. Mehregany, IEEE Trans. Electron Devices **60**, 513 (2013).
[5] Y. H. Zhu, J. C. Zhang, Z. T. Chen, and T. Egawa, J. Appl. Phys. **106**, 124506 (2009).
[6] M. Suemitsu, Y. Miyamoto, H. Handa, and A. Konno, e-Journal Surf. Sci. Nanotechnol. **7**, 311 (2009).
[7] R. Yakimova, R. Vasiliauskas, J. Eriksson, and M. Syväjärvi, Mater. Sci. Forum **711**, 3 (2012).
[8] D. Morelli, J. Heremans, C. Beetz, W. Woo, G. Harris, and C. Taylor, Instit. Phys.: Conf. Ser. **137**, 313 (1994).
[9] J. R. Jenny, D. P. Malta, S. G. Müller, A. R. Powell, V. F. Tsvetkov, H. M. Hobgood, R. C. Glass, and C. H. Carter, J. Electron. Mater. **32**, 432 (2003).
[10] G. A. Slack, J. Appl. Phys. **35**, 3460 (1964).
[11] H. P. Phan, D. Viet Dao, P. Tanner, L. Wang, N. T. Nguyen, Y. Zhu, and S. Dimitrijev, Appl. Phys. Lett. **104**, 111905 (2014).
[12] B. Liao, B. Qiu, J. Zhou, S. Huberman, K. Esfarjani, and G. Chen, Phys. Rev. Lett. **114**, 115901 (2015).
[13] B. Liao, A. A. Maznev, K. A. Nelson, and G. Chen, Nat. Commun. **7**, 13174 (2016).
[14] N. Mingo, D. A. Stewart, D. A. Broido, L. Lindsay, and W. Li, in *Length-Scale Dependent Phonon Interactions*, edited by L. S. Shindé and P. G. Srivastava (Springer, New York,, 2014), pp. 137–173.
[15] P. Hohenberg and W. Kohn, Phys. Rev. **136**, B864 (1964).
[16] W. Kohn and L. J. Sham, Phys. Rev. **140**, A1133 (1965).
[17] S. Baroni, P. Giannozzi, and A. Testa, Phys. Rev. Lett. **58**, 1861 (1987).
[18] X. Gonze, Phys. Rev. A **52**, 1086 (1995).
[19] W. Li, J. Carrete, N. A. Katcho, and N. Mingo, Comput. Phys. Commun. **185**, 1747 (2014).
[20] M. Berglund and M. E. Wieser, Pure Appl. Chem. **83**, 397 (2011).
[21] J. M. Ziman, *Electrons and Phonons: The Theory of Transport Phenomena in Solids*, International series of monographs on physics (Oxford University Press, Oxford, 1960).
[22] F. Giustino, Rev. Mod. Phys. **89**, 015003 (2017).
[23] S. Poncé, E. Margine, C. Verdi, and F. Giustino, Comput. Phys. Commun. **209**, 116 (2016).
[24] N. Marzari, A. A. Mostofi, J. R. Yates, I. Souza, and D. Vanderbilt, Rev. Mod. Phys. **84**, 1419 (2012).
[25] F. Giustino, M. L. Cohen, and S. G. Louie, Phys. Rev. B **76**, 165108 (2007).
[26] P. Giannozzi, S. Baroni, N. Bonini, M. Calandra, R. Car, C. Cavazzoni, D. Ceresoli, G. L. Chiarotti, M. Cococcioni, I. Dabo, A. Dal Corso, S. de Gironcoli, S. Fabris, G. Fratesi, R. Gebauer, U. Gerstmann, C. Gougoussis, A. Kokalj, M. Lazzeri, L. Martin-Samos, N. Marzari, F. Mauri, R. Mazzarello, S. Paolini, A. Pasquarello, L. Paulatto, C. Sbraccia, S. Scandolo, G. Sclauzero, A. P. Seitsonen, A. Smogunov, P. Umari, and R. M. Wentzcovitch, J. Phys. Condens. Matter **21**, 395502 (2009).
[27] J. P. Perdew and A. Zunger, Phys. Rev. B **23**, 5048 (1981).

[28] N. Troullier and J. L. Martins, Phys. Rev. B **43**, 8861 (1991).
[29] A. Taylor and R. M. Jones, *Proceedings of the Conference on Silicon Carbide (Boston, MA 1959)*, edited by J. O'Connor and J. Smiltens (Pergamon, New York, 1960), pp. 147–154.
[30] J. P. Perdew, K. Burke, and M. Ernzerhof, Phys. Rev. Lett. **77**, 3865 (1996).
[31] J. Serrano, J. Strempfer, M. Cardona, M. Schwoerer-Bhning, H. Requardt, M. Lorenzen, B. Stojetz, P. Pavone, and W. J. Choyke, Appl. Phys. Lett. **80**, 4360 (2002).
[32] F. Widulle, T. Ruf, O. Buresch, A. Debernardi, and M. Cardona, Phys. Rev. Lett. **82**, 3089 (1999).
[33] Y. Goldberg, M. Levinshtein, and S. Rumyantsev, *Properties of Advances in Semiconducting Materials GaN, AIN, InN, BN, SiC, SiGe*, edited by M. E. Levinshtein, S. L. Rumyantsev, and M. S. Shur (John Wiley & Sons, New York, 2001), Chap. 5, p. 94.
[34] R. Taylor, H. Groot, and J. Ferrier, *TRPL 1336, Thermophysical Properties Research Laboratory Report* (Purdue University, 1993).
[35] L. Lindsay, D. A. Broido, and T. L. Reinecke, Phys. Rev. B **87**, 165201 (2013).
[36] A. Katre, J. Carrete, B. Dongre, G. K. H. Madsen, and N. Mingo, Phys. Rev. Lett. (to be published).
[37] C. Persson and U. Lindefelt, Phys. Rev. B **54**, 10257 (1996).
[38] N. H. Protik, A. Katre, L. Lindsay, N. Mingo, and D. Broido, Mater. Today Phys. **1**, 31 (2017).